Sedimentary evidence of deglacial megafloods in the northern Gulf of Mexico (Pigmy Basin)

Jean Carlos Montero-Serrano, Viviane Bout-roumazeilles, Nicolas Tribovillard, Thomas Sionneau, Armelle Riboulleau, Aloys Bory, Benjamin Flower

Sedimentary evidence of deglacial megafloods in the northern Gulf of Mexico (Pigmy Basin)

Jean Carlos Montero-Serrano [a],*, Viviane Bout-Roumazeilles [a], Nicolas Tribovillard [a],Thomas Sionneau [a], Armelle Riboulleau [a], Aloys Bory [a], Benjamin Flower [b]

[a] Université Lille 1, Laboratoire Géosystèmes, UMR 8157 CNRS, bâtiment SN5, 59655 Villeneuve d'Ascq cedex, France

[b] College of Marine Science, University of South Florida, 140 7th Avenue South, St. Petersburg, FL 33701, USA

Email addresses : jc.montero-serrano@ed.univ-lille1.fr (J.C. Montero-Serrano), viviane.bout@univ-lille1.fr (V. Bout-Roumazeilles), nicolas.tribovillard@univ-lille1.fr (N. Tribovillard), sionneau.thomas@wanadoo.fr (T. Sionneau), armelle.riboulleau@univ-lille1.fr (A. Riboulleau), aloys.bory@univ-lille1.fr (A. Bory).

Corresponding author: J.C. Montero-Serrano. Tel.: +33 320434395; fax: +33 320434910.

Abstract.

Cored sediments from the Pigmy Basin, northern Gulf of Mexico, were analyzed in order to better constrain late deglacial and early Holocene paleoenvironmental and sedimentary changes in response to North American climate evolution. Mineralogical and geochemical proxies indicate the succession of two sedimentary regimes: dominantly detrital during the deglaciation (15–12.9 cal ka BP) whereas biogenic contribution relatively increased later on during the Younger Dryas and early Holocene (12.9 and 10 cal ka BP). Geochemical data reveal that the deglacial record mainly reflects variations of terrigenous supply via the Mississippi River rather than modifications of redox conditions in the basin. Specific variations of almost all the parameters measured in this paper are synchronous with the main deglacial meltwater episode (Meltwater Spike) described or modeled in previous marine or continental studies. During this episode, most parameters display ‘‘stair-step-like’’ – pattern variations highlighting three successive steps within the main meltwater flow. Variations in grain-size and clay mineral assemblage recorded in the Pigmy Basin indicate that the erosional regime was very strong on land during the first part of the Meltwater Spike, and then milder, inducing more subtle modifications in the sedimentary regime in this part of the Gulf. Specific geochemical and mineralogical signatures (notably, clay minerals and trace metal geochemistry) pinpoint a dominant origin from NW North America for detrital particles reflecting meltwater outflow from the south-western Laurentide Ice Sheet (LIS) margin

during the most intense freshwater discharge. The observed decrease of the sedimentation rate from about 200 to 25 cm/ka at ca 12.9 ka evidenced a drastic decrease of erosional processes during late phase of discharge, consistently with the hypotheses of major reduction of meltwater flow. The major modification at 12.9 cal ka BP is interpreted to result from both modifications of the main Mississippi fluvial regime due to eastward and northward rerouting of meltwater flow at the onset of the Younger Dryas, and the increase of sea-surface temperature linked to insolation. Finally, slight grain-size modifications suggest that some freshwater discharges may have episodically reached the Gulf of Mexico after the Younger Dryas reflecting possible small adjustments of the postglacial hydrological regime.

Keywords: Gulf of Mexico, Pigmy Basin, Laurentide Ice Sheet, deglaciation, early Holocene, meltwater floods, Mississippi River.

1. Introduction

It has long been known that the hydrological features of the Gulf of Mexico (GOM) were strongly impacted by the inputs of meltwater from the Laurentide Ice Sheet (LIS) during the last glacial cycle and subsequent deglaciation, since the Mississippi/Missouri watershed represented the main drainage system for the southern LIS meltwater (Kennett and Shackleton, 1975; Leventer et al., 1982; Joyce et al., 1993; Aharon, 2003; Flower et al., 2004). Deglacial meltwater episodes have been extensively documented in the GOM using hydrological proxies (Kennett and Shackleton, 1975; Emiliani et al., 1978; Leventer et al., 1982; Broecker et al., 1989; Flower and Kennett, 1990; Spero and Williams, 1990; Marchitto and Wei, 1995; Aharon, 2003; Flower et al., 2004). Modeling estimates indicate that the water discharge through the Mississippi River has varied by a factor of 5 during the Lateglacial (Teller, 1990), reflecting both the melting history of the LIS and also possible modifications in meltwater drainage pathways. Paleogeographic and ice sheet volume reconstructions suggest that some of the ice lobe-extent Reconstructions suggest that during deglaciation the ice-lobe fluctuations during deglaciation resulted in rapid switches of the meltwater flows pathways from the Mississippi River drainage towards the eastern drainage systems, triggering episodic cooling and warming in the North Atlantic region (Licciardi et al., 1999; Clark et al., 2001).

On the other hand, the detrital sedimentary record (including organic matter sources) of these meltwater discharges within the GOM has been studied in different works, for example in: (a) Orca Basin (Marchitto andWei, 1995; Brown and Kennett, 1998; Meckler et al., 2008; Sionneau et al., 2008, in revision); (b) Pigmy Basin (Jasper and Gagosian, 1989a, b, 1990; Jasper and Hayes, 1993); and (c) Bryant Canyon (Tripsanas et al., 2007). An important aspect to extract of these studies is that the mineralogy, geochemistry and nature of the terrigenous components transported by the Mississippi River toward the GOM during the meltwater discharges are characteristics of the drainage areas, where the bedrock/soils contain both different clay mineral assemblages (Brown and Kennett, 1998; Sionneau et al., 2008, in revision) and geochemical signatures (Gustavsson et al., 2001). Indeed the mineralogical nature of sediments directly depends on the petrographic characteristics of their source areas (e.g., Bout-Roumazeilles et al., 1999; Sionneau et al., 2008) and they are useful to reconstruct the variability of detrital provenance through time if their main sources are well identified and constrained.

The northern GOM (Fig. 1a) is composed of small intraslope basins (e.g., Pigmy, Orca, La Salle basins) where sedimentation is mainly controlled by terrigenous supply from the Mississippi River and may record specific detrital discharges associated with the LIS melting history (Bout-Roumazeilles and Trentesaux, 2007). In this paper, we report on sedimentological and geochemical variations in terrigenous inputs in core MD02-2553 from the Pigmy Basin in the GOM during the last deglaciation. We chose the Pigmy Basin because it is located at some distance from the Mississippi Delta system. Thus, it collects continuously a smoothed and averaged terrigenous supply from North America and avoids local perturbations linked to the Louisiana slope depositional processes (Aharon, 2003, 2006). Using multiproxy analyses (grain-size, clay mineralogy, magnetic susceptibility, elemental analysis, inorganic geochemistry) on the deglacial terrigenous record of the Pigmy Basin, we aim to determine in detail the timing of continental erosion and sedimentary provenance of the main meltwater discharges, in order to: (1) document the different melting phases of the southern edge of the LIS; and (2) better constrain the history of meltwater input and its terrigenous transfers into the GOM.

2. Pigmy basin – geological framework

The Pigmy Basin is located on the Louisiana continental slope, about 250 km southwest of the present-day Mississippi Delta, in the northern GOM. The basin is approximately 20 km-long, 7 kmwide, with average depth of 2300 m (Fig. 1b). The structure and bathymetry of the slope are controlled mainly by salt tectonics (Bouma, 1981), with salt domes protruding several hundred meters about the interdiapiric sea floor (Fig.1b). The Pigmy Basin is defined as a former channel dammed by diapirs, with infilling by bottom transport. Thus sedimentation in the basin is mainly hemipelagic and is strongly linked to the Mississippi River detrital supply (Bouma and Coleman, 1986).

Studies from the Deep-Sea Drilling Project site 619 (Leg 96, Pigmy Basin, Fig. 1b) revealed that the Holocene section displays some intervals nearly devoid of foraminifera. These observations suggest high dilution of the faunal content by rapid influx of terrigenous sediments (Schroeder, 1983; Kohl et al., 1985). Sedimentation rates are higher during glacial isotopic stages (200–300 cm/ka) than during interglacial stages and substages (71–92 cm/ka) because of both increased physical erosion onshore and low sea level characterizing glacial periods. Coleman (1988) evidenced some variability in sediment accumulation during the Holocene, probably resulting from the migration of the main Mississippi River Delta.

Previous studies on the Pigmy Basin revealed glacial–interglacial variability in both the clay composition and terrigenous organic supply (e.g., Tieh et al., 1983; Jasper and Gagosian, 1989a, b, 1990; Jasper and Hayes, 1993). These observations suggest that this major mineral or/and organic terrigenous supply linked to meltwater discharge from the LIS during the deglaciation may have imprinted the Pigmy Basin sedimentary record.

3. Materials and methods

3.1. Materials

The samples were taken from the 10.3 m long core MD02-2553 (Calypso Square). The core was collected in the Pigmy Basin (27°11.01 N, 91°25.00 W) close to DSDP Site 619 (Leg 96, Bouma et al., 1986) during the 2002 Paleoceanography of the Atlantic and Geochemistry (PAGE) cruise of the research vessel Marion Dufresne, as part of the International Marine Past Global Changes Study (IMAGES) program (Fig. 1b). The sediment is mainly composed of massive or faintly laminated greenish gray to dark greenish gray silty to clayey mud throughout the core (Fig. 1c). Slight bioturbation is observed in the sediments. The uppermost 155 cm of the core are composed of sandy to silty clay with foraminifers and

coccoliths, whereas the lower part is made up with clays showing foraminifers that become scarce below 400 cm. Dark micro laminations (mm- to cm-scale) are observed between 625–655, 880–946, and 981–1030 cm (Fig. 1c). A homogeneous interval is observed between 655 and 860 cm of the core. Five distinct upward grading, foraminifer-rich, sandy layers interpreted as small turbidites (Meckler, 2006) occurring in the core (298–300, 399–400, 594–596, 614–615, and 974–984 cm). These small turbidites were removed from our calculations because they do correspond to instantaneous processes and will distort the stratigraphic distribution of the proxies (age model).

For this study, the core was evenly sampled every 5 cm between 354 and 1029 cm (yielding a total of 139 samples); this interval corresponds to the deglacial section of the core (see Section 3.2 below). Aliquots of the homogenized sediment samples were rinsed five times to remove salt, dried (40 °C for 48 h) and ground for magnetic susceptibility and geochemical analysis.

3.2. Age model

The chronology of the core MD02-2553 is determined from seven accelerator mass spectrometry (AMS) 14C dates on foraminifera on the studied interval (354–1029 cm) (Table 1; gray dots in Fig. 2). The younger five dates were measured on mixed planktic foraminifers at the CAMS, Lawrence Livermore National Laboratory, USA (Poore et al., in press). The other dates were measured on monospecific Globigerinoides ruber (both pink and white varieties) at the Poznan Radiocarbon Laboratory, Poland. All ages were converted into calendar years with the CALIB software (Stuiver and Reimer, 1993, version 5.0.2; http://calib.qub.ac.uk/calib), using thecalibration curve Marine04 (Hughen et al., 2004). All AMS 14C ages were corrected using a constant reservoir age of 400 years ($\Delta R = 0$) because it provides consistency with both modern values (Bard, 1988) and with previous paleoceanographic studies from the GOM (e.g., Flower et al., 2004; Meckler et al., 2008; Nu¨ rnberg et al., 2008). Reservoir age modifications in the tropical Atlantic Ocean during Late Pleistocene and Holocene are still a matter of debate (Stocker and Wright, 1996; Ru¨ hlemann et al., 2004). However a detailed study of Hughen et al. (1998) indicates that reservoir ages did not change significantly during the last deglaciation. Depth in centimeters was converted to calendar age by linear interpolation between four main calibrated AMS 14C ages at 350.5, 424.5, 640, and 932 cm (black squares in Fig. 2). Linear extrapolation from the radiocarbon

160 date suggests that the age of the core base is approximately 15.1 cal ka BP. Age vs. depth
161 relations in the core MD02- 2553 indicate linear sedimentation rates ranging from about 200
162 to 397 cm/ka during the last deglaciation and a significant drop to values of about 25 cm/ka
163 during the early Holocene (dotted line with black squares in Fig. 2). These values are in good
164 agreement with sedimentation rates obtained on: (1) DSDP site 619 of the Pigmy Basin: 300
165 cm/ka in stage 2 and 92 cm/ka in stage 1 (Jasper and Gagosian, 1990); and (2) core MD02-
166 2552 of the Orca Basin: ca 215 cm/ka during the last deglaciation and ca 65 cm/ka during the
167 early Holocene (Sionneau et al., in revision). The distinct increases in linear sedimentation
168 rates from about 25 to 397 cm/ka at about 12.9, 14, and 14.7 ka appear very large and abrupt,
169 following a stairstep pattern; however, the accumulation is thought to have been continuous
170 because of the lack of sharp lithological breaks or sedimentological indicators of hiatus or
171 mass flow transport in these parts of the core. In addition, the decrease in sedimentation rates
172 from 200 to 25 cm/ka at ca 12.9 ka is consistent with major reduction of meltwater flow
173 (Licciardi et al., 1999; Tarasov and Peltier, 2005; Teller et al., 2005).

174

175 **3.3 Analytical methods**

176 *3.3.1. Grain size distribution*

177 Grain-size determination was carried out on the carbonate-free fraction of the
178 sediment using a Malvern Mastersizer 2000 laser diffractometer, which has a detection range
179 of 0.02–2000 mm. Sample preparation and optical settings for the Mastersizer 2000 followed
180 Sperazza et al. (2004). Defloculation of the samples was done by successive washing with
181 distilled water after decarbonatation of the sediments with 0.2 M HCl. Samples were split
182 with a 2000 rpm stirrer and disaggregated by 40% ultrasonication (Hydro S dispersion cell)
183 for >60 s during analysis. Sample quantity was adjusted in order to obtain a laser beam
184 obscuration between 12 and 15%. We used a refractive index (RI) value of 1.544 (quartz) and
185 an absorption value of 0.05. The distribution parameters reported here are the mode (mm,
186 most frequent grain-size) and percentage of clays (<2 mm), cohesive-silts (2–10 mm),
187 sortable-silts (10–63 mm) and sands (>63 mm).

188

189 *3.3.2. Clay mineral analysis*

190 Clay mineral associations were studied using X-ray diffraction following the protocol
191 of Bout-Roumazeilles et al. (1999). In this paper, ‘‘clay minerals’’ refer to the major

192 phyllosilicate minerals within the clay-size fraction (generally less than 2-mmparticles). All
193 samples were first decalcified with 0.2 MHCl. Defloculation of clays was achieved by
194 successive washing with distilled water. The claysize fraction was separated by settling
195 according to Stokes's law, concentrated by centrifugation, and oriented by wet smearing on
196 glass slides. X-ray diagrams were obtained using a Philips PW 1749 diffractometer with
197 CuKa radiation and a Ni filter. A tube voltage of 40 kV and a tube current of 25 mA were
198 utilised. Three X-ray diagrams were performed: air-dried sample (normal run), ethylene–
199 glycol vapour saturation for 12 h (glycol run) and heating at 490 °C during 2 h (heating run).
200 The goniometer scanned from 2.49° to 32.49° 2Θ for normal and glycol run and from 2.49° to
201 14.5° 2q heating run. Each clay mineral is characterized by its basal layer plus interlayer
202 interval (d) as revealed by XRD analysis (Brown and Brindley, 1980). Smectite (S) is
203 characterized by a peak at 14 Å on the normal run, which expands to 17 Å after saturation by
204 ethylene–glycol and retracts to 10 Å after heating. Illite (I) presents a basal peak at 10 Å on
205 the three runs. Chlorite (C) is characterized by peaks at 14 Å (001), 7 Å (002), 4.75 Å (003)
206 and 3.53 Å (004) on the three runs. Kaolinite (K) is characterized by peaks at 7 Å (001) and
207 3.58 Å (002) on the normal and glycol runs. Both peaks disappear or are strongly reduced
208 after heating. To distinguish kaolinite from chlorite, the portion of the spectrum containing
209 the basal peaks of kaolinite (002) and chlorite (004) around 3.55 Å is step-scanned in a high-
210 resolution mode following standard procedures described in detail by Petschick et al. (1996).
211 Semiquantitative estimation of clay mineral abundances is based on peak areas and summed
212 to 100% (S + I + K + C 1/4 100%). Peak area measurements were realized in the glycol runs
213 using the Macintosh MacDiff® 4.2.5 software (Petschick, 2000). The error on the
214 reproducibility of measurements is estimated to be ±5% for each clay mineral.

215

216 *3.3.3. Rock-Eval pyrolysis*

217 Usual Rock–Eval pyrolysis parameters, namely, total organic carbon content (TOC,
218 wt.%), Tmax (°C), and Hydrogen Index (HI, in mg hydrocarbon per g TOC) were determined
219 with a Delsi Oil Show Analyser (Rock Eval II). The pyrolysis program was adapted to recent
220 sediments, starting with an isothermal stage of 3 min at 180 °C. Then, the pyrolysis oven
221 temperature was raised at 30 °C/ min to 600 °C, and held for 3 min at this temperature (see
222 Espitalié et al., 1986 for procedural details and Disnar et al., 2008 for Rock– Eval use for
223 Holocene sediments).

224

225 *3.2.4. Elemental analysis*

226 Total inorganic carbon (TIC) content was determined as calcium carbonate (CaCO3)
227 percentage using a Bernard calcimeter (measuring the amount of CO2 released by acid
228 digestion, and based on standard samples of pure CaCO3 – precision <5%).

229 Total sulfur (S_{total}) and total nitrogen (Ntotal) contents were determined using a
230 Thermo Flash EA1112 CHNSO analyser. The precision is better than 4% for S_{total} and 5% for
231 Ntotal, based on international standards and replicate samples. Though nitrogen may be
232 present in the form of nitrate or ammonium in clay minerals, it is estimated that Ntotal mostly
233 corresponds to organic nitrogen. With this assumption, the C/N ratio (TOC/Ntotal) was
234 calculated as an indication of source of organic matter (OM) in sediments (Jasper and
235 Gagosian, 1990; Meyers, 1997; Meckler et al., 2008). C/N ratio values for organic matter
236 (OM) of marine origin generally range from 4 to 10 because of the high protein content of
237 lower organisms such as phytoplankton and zooplankton (e.g., Meyers, 1997). Higher plant-
238 derived OM gives higher C/N values than those of marine origin OM because it has a high
239 percentage of non-protein materials (e.g., C/N > 15; Meyers, 1997).

240

241 *3.2.5. Magnetic susceptibility*

242 Magnetic susceptibility (MS) was measured on all discrete samples, using a KLF-4
243 Agico apparatus. Remnantmagnetizationwas measured on the three-axis using a magnetic
244 field of 300 A/m with a step of 10 A/m. Each sample was measured three times and the mean
245 of these measurements is reported here. MS is normalized by dry mass and expressed as
246 m3/kg. In Pigmy Basin, the MS measurements are useful for detecting paleoenvironmental
247 changes induced in the magnetic properties of marine sediments (King, 1986).

248

249 *3.3.6. Inorganic geochemistry*

250 Major, minor, trace and rare earth elements (REE) concentrations were determined on
251 35 evenly distributed samples (average sample spacing is ~20 cm) by inductively coupled
252 plasma optical emission spectrometry (ICP-OES) and inductively coupled plasma mass
253 spectrometry (ICP-MS), at Activation Laboratories Ltd. (Ancaster, Canada). Samples were
254 mixed with a flux of lithium metaborate (LiBO2) and lithium tetraborate (Li2B4O7), and

fused in an induction furnace. Molten sample was immediately poured into a solution of 5% nitric acid (HNO3) containing an internal standard, and mixed continuously until completely dissolved. The analytical accuracy and precisionwere found to be better than 1–2% for major elements, 5% for REE and 5–10% for the other elements, as checked by international standards and analysis of replicate samples.

Elemental compositions and total REE are normalized to aluminum (Al) to remove the effects of differential dilution of the bulk sediments by the aluminosilicate fraction so that changes in the composition of the lithogenous material can be discerned (see discussion about Al normalization in van der Weijden, 2002, and Tribovillard et al., 2006). In addition, trace metal (TM) concentrations are expressed in terms of enrichment factors (EFTM) where the Al-normalized metal concentration is compared to the average shale values of Wedepohl (1971, 1991): EFTM = TM/Al_{sample}: TM/ $Al_{average}$ shale. EFTM > 1 suggests enrichment relative to average shale but authigenic enrichments can be suspected when EF_{TM} exceed 5 (Tribovillard et al., 2006). Fractionation between light REE (LREE: La–Nd), medium REE (MREE: Sm–Gd) and heavy REE (HREE: Tb–Lu) was studied by La/Yb and Gd/Yb normalized ratios (Lawrence et al., 2006). Additionally we calculated the distribution of Ce-anomaly (3Cen: 2Lan + Ndn) and Eu-anomaly [Eun: $(Sm_n.Gd_n)1/2$] to studied vertical changes in redox conditions. NASC values by Gromet et al. (1984) are used for normalization of the REE.

Al-normalized metal distributions are used as proxies of the detrital sediment sources, complementary to clay mineral proxies. In addition, the REE abundance patterns provide fingerprints associated with detrital fraction of the sediment which in turn represents the bulk composition and stands as proxy for the climate over the source area (e.g., Tanaka et al., 2007).

4. Results

Four main sedimentary units can be identified on the base of the characteristic stair-step patterns of most sedimentological and geochemical proxies (Fig. 3–9). The characteristic stair-step pattern possibly displays the effect of highly variable sedimentation rates (25–397 cm/ka) in Pigmy Basin, and may reveal differences due to clastic dilution and provenance. However, it is necessary to take into consideration that age control rests on interpolation between 14C dates. These units, labelled 1–4 frombase to top, are described below.

287

288 *4.1. Unit 1: 1029–920 cm (15–14.7 cal ka BP)*

289 This unit is mainly characterized by coarsest mode values (ca. 3.8 mm). The
290 proportion of sortable (non-cohesive) silts displays the maximum values of the whole studied
291 interval whereas the fine-cohesive fraction is minimum (Fig. 3). Although smectite is the
292 main component of the clay mineral fraction (ca. 70%), Unit 1 is characterized by enhanced
293 contributions of illite (up to 17%), kaolinite (up to 11%) and chlorite (up to 10%) (Fig. 4).
294 The unit is characterized by intermediate values of TOC associated with a low S_{total} content
295 (Fig. 5). The CaCO3 content (Fig. 5) is slightly higher than average (up to 13%). Unit 1
296 displays relatively high Ti/Al and K/Al values and low Fe/Al and V/Al (Fig. 9)

297

298 *4.2. Unit 2: 920–640 cm (14.7–14 cal ka BP)*

299 Unit 2 is characterized by specific sedimentological and geochemical characteristics
300 with low internal variability, associated with a very high sedimentation rate (397 cm/ka). The
301 mode is quite low (down to 3.1 mm) reflecting a high contribution of cohesive particles (up to
302 95%), whereas MS and CaCO3 content display their lowest values (Figs. 3 and 5). The clay
303 assemblage is markedly dominated by smectite (up to 86%) (Fig. 4). It may be emphasized
304 that the domination of smectite does not result from differential settling processes (Sionneau
305 et al., 2008). High TOC (up to 1.7%) and S_{total} (0.10%) contents and high C/N ratios underline
306 the specificity of Unit 2 (Fig. 5). Moreover the geochemical signature of Unit 2 differs
307 drastically from the other three units. The most remarkable feature is the high V/Al and Fe/Al
308 values associated with depressed values of K/Al, Ti/Al, Th/Al, and depletion in most REE
309 (Fig. 9). The peculiar geochemical character of this unit is also obvious on Ti/Al vs. Fe/Al or
310 Th/Al vs. V/Al plots (Fig. 8a,b). Fig. 8c shows that the relatively high contents in V are still
311 strongly correlated to Al concentrations, which points to a terrigenous origin. In addition
312 (La/Yb)n and (Gd/Yb)n ratios show a slight enrichment in LREE and MREE over HREE
313 (Fig. 9).

314

315 *4.3. Unit 3: 640–424 cm (14–12.9 cal ka BP)*

316 Most geochemical and sedimentological characteristics of this unit are very similar to
317 Unit 1, except for grain-size and CaCO3 distributions that are similar to those of Unit 2 (Figs.

3–9). Some minor discrepancies between Unit 3 and Unit 1 may however be observed: a slightly coarser mode and higher proportion of sortable- silt at the base of Unit 3. Unit 3 is also characterized by an increase of the (La/Yb)n ratio, reflecting slightly enhanced fractionation of LREE (Fig. 9). The sedimentation rate is still high (200 cm/ka) though lower than in Unit 2.

4.4. Unit 4: 424–354 cm (12.9–10 cal ka BP)

The strong decrease of the sedimentation rate is the most prominent feature of Unit 4, also characterized by the increase in grain-size mode and CaCO3 content (up to 22%) (Figs. 3 and 5). The clay fraction is characterized by the increased contribution of illite (up to 15%), kaolinite (up to 12%) and chlorite (up to 10%) at the expense of smectite (Fig. 4). The TOC concentrations and C/N ratio values display a decreasing trend over the interval whereas the S_{total} content is steadily low (Fig. 5). Geochemical parameters would not provide any significant information because elemental analyses were performed only on three samples.

5. Interpretation and discussion

5.1. Main characteristics of sedimentary regimes in the Pigmy Basin

Our mineralogical and geochemical results indicate that sedimentation in the Pigmy Basin is mainly ruled by the terrigenous supply over the entire interval (Figs. 3–9) being strictly detrital during the deglaciation (Units 1–3) whereas significant biogenic contribution is observed during the Younger Dryas and early Holocene (Unit 4).

Geochemical proxies highlight a dominant detrital signature and a non-detectable influence of authigenic and diagenetic processes in the Pigmy Basin. Element enrichment factors do not show any significant variations (average, 0.5–2.5), which also indicates that the redox sensitive and/or sulfide-forming trace metals (e.g., V, U, Mo, Cu, Ni, Co) are not authigenically enriched (EFTM < 5) (Fig. 7). Accordingly, these trace metals show good correlation with Al concentrations, advocating to a detrital origin (e.g., Fig. 8c). REE normalized patterns, and Ce and Eu anomalies do not show any striking features, except for a general slight enrichment in light REE over HREE evidenced by the (La/Yb)n and (Gd/Yb)n (Fig. 9). The absence of any significant fractionation of REE in the Pigmy Basinsediments, also observed in other basins from the GOM (Flocks and Swarzenski, 2007), points out a

highly-mixed detrital source. These results confirm that the terrigenous supply from the Mississippi and Missouri rivers, draining almost half the conterminous USA, mostly controls sedimentation in the GOM. Moreover similar REE distributions are observed in the Pigmy Basin and in Mississippi River suspended loads (Goldstein and Jacobsen, 1988; Elderfield et al., 1990) confirming the dominant influence of the Mississippi River and minor contributions of Mobile, Brazos and Atchtalafaya rivers.

Complementarily, the C/N ratio (up to 15; Fig. 5) and Rock–Eval parameters (Fig. 6) also suggest that organic compounds are mostly of terrigenous origin during the deglaciation whereas they display a higher marine influence in the early Holocene (Unit 4); the samples of Unit 4 show relatively high HI and low Tmax values (Fig. 6b). In addition as indicated by a Tmax vs. HI diagram (Fig. 6a), the studied core contains an immature of type-III OM (terrestrial OM). These observations are in agreement with previous studies on the OM of the Pigmy Basin (Jasper and Gagosian, 1990) and the nearby Orca Basin (Meckler et al., 2008; Tribovillard et al., 2008, 2009; Sionneau et al., in revision).

Under this frame, any variation in the Pigmy Basin sedimentation is then likely to result from modifications of the Mississippi River flow that is largely controlled by meltwater discharges from the LIS during the deglaciation (Fig. 10c, Licciardi et al., 1999).

Several studies provide a detailed record of meltwater discharges in the GOM for the past 20 ka (Marchitto andWei, 1995; Brown and Kennett, 1998; Aharon, 2003, 2006; Flower et al., 2004; Meckler et al., 2008). Reconstructions suggest that during the Last Glacial Maximum (LGM) most meltwaters originated from the central LIS and were further drained toward the GOM via the Mississippi River (Teller, 1990; Licciardi et al., 1999). On the contrary, during deglaciation ice sheet margin instability and ice lobe fluctuations modified meltwater provenance and caused the main drainage to be repeatedly rerouted eastward (toward the North Atlantic Ocean) or northward (toward the Arctic Ocean). As a consequence discharge fluctuations display different regimes (Teller, 1990; Licciardi et al., 1999) and have likely affected also the provenance of detrital particles (Sionneau et al., in revision).

Over the studied interval, two periods of freshwater discharge are evidenced in d18O profiles. The first major discharge occurred during the last deglaciation between 16.5 and 13 cal ka BP as a series of freshwater pulses attributed to the release of glacial meltwater from proglacial Great Lakes and Lake Agassiz (Aharon, 2003; Lewis and Teller, 2006). A minor

discharge may have occurred during early Holocene to the GOM resulting from the release of meltwater from Lake Agassiz at 11.4–10.6 cal ka BP (Tripsanas et al., 2007).

In this context, our mineralogical and geochemical results provide new insights the expression of these meltwater episodes in the GOM. A recent study (Sionneau et al., in revision) proposed the use of clay mineralogy to retrace meltwater provenance. Indeed during the last deglaciation, the south margin of the LIS and proglacial lakes encompassed two distinct clay mineral provinces (Fig. 1a). The north-western Mississippi and Missouri river watershed is characterized by high smectite contents, which reflect the composition of Cretaceous, Tertiary and Pleistocene bedrocks associated with a bentonitic or authigenic origin (Sionneau et al., 2008). On the other hand, the northeastern province corresponding to the Great Lakes area and the Ohio and Tennessee river catchment mainly delivers illite and chlorite, resulting from strong physical weathering and erosion of Palaeozoic rocks (Sionneau et al., 2008). The respective contributions of smectite vs. illite and chlorite are thus used to document the origin of deglacial meltwater megafloods (Sionneau et al., in revision).

5.2. The main meltwater discharge episode (15–12.9 cal ka BP)

Previous studies based on deep-sea cores from the GOM (Leventer et al., 1983; Jasper and Gagosian, 1989a, b, 1990; Jasper and Hayes, 1993; Marchitto and Wei, 1995; Brown and Kennett, 1998; Aharon, 2003; Flower et al., 2004; Meckler et al., 2008) and on continental records from North America (e.g., Knox,1996; Rittenour et al., 2007) evidenced the occurrence of a modest multi-phased surge of glacial meltwater during deglaciation (Figs.10 and 11). This episode is defined by a major negative d18O excursion (-2.5‰) between 15.2 and 13 cal ka BP referred to as the Meltwater Spike (Fig. 11a, Leventer et al., 1983; Brown and Kennett, 1998; Flower et al., 2004) and meltwater pulse (MWP-1a) (Fig. 10b, Tarasov and Peltier, 2005) in the GOM, and to meltwater flow (MWF)-3 and MWF-4 on the Louisiana Slope (Fig. 11b, Aharon, 2003).

The sedimentological Units 1–3 defined on core MD02-2553 are synchronous with this Meltwater Spike. The peculiar stair-step pattern of most sedimentological and geochemical proxies provides additional constrains on the synopsis of this major meltwater episode. Our results show that the Meltwater Spike corresponds to three stair-step terrigenous inputs (Units 1–3) with a maximum discharge leading to the deposition of Unit 2 (14.7 and 14

411 cal ka BP). These three phases are characterized in the Pigmy Basin sediments by distinct
412 mineralogical and geochemical signatures.

413 In core MD02-2553, the Meltwater Spike is marked by relatively elevated TOC (0.7–
414 1.5%) and S_{total} (0.06–0.18%) concentrations, and high C/N ratio (9.5–22.7) (Fig. 5)
415 consistent with previous observations on the nearby Orca Basin, core MD02-2550 (see Fig. 5
416 of Meckler et al., 2008). It is noticed that that in spite of the independent age models of the
417 two nearby cores MD02-2553 and MD02-2550, the changes in TOC and C/N distributions for
418 both cores are of the same order (in time and magnitude) with the most pronounced increase
419 in meltwater flux reflected by d18O (-2.5‰). The results of this correlation provide strong
420 support to our interpretations.

421 Concurrently, the peculiar grain-size distribution characterizing Unit 1 indicates
422 specific supply of coarse particles. Mineralogical and geochemical proxies indicate a mixed
423 provenance of detrital particles, i.e., mainly from the north-western province but with some
424 noticeable contribution of the northeastern province. These results suggest that the Mississippi
425 River received almost all meltwaters from the southwest of James glacial lobe to the eastern
426 margin of Lake Erie (Sionneau, 2008) during the early phase of the Meltwater Spike (Fig. 1a).
427 According to these observations, the deposition of Unit 1 is likely resulting from erosion of
428 the main braided Mississippi River channel rather than from clay-rich terrace deposits along
429 tributaries (Knox, 1996). Our results suggest that Unit 1 may record the initial erosive flood
430 corresponding to the proglacial Lake Wisconsin outburst that occurred at 14.9 cal ka BP (Fig.
431 1a, Knox, 1996).

432 Unit 2 displays rather characteristic mineralogical and geochemical compositions: the
433 detrital fraction is typically finegrained, enriched in smectite and detrital organic matter, and
434 exhibits a peculiar geochemical signature. These characteristics highlight modifications of
435 provenance of the main detrital supply. The clay composition – enriched in smectite at the
436 expense of both illite and chlorite (Fig.11f,h) – suggests a westward shift of the main outflow
437 from the Great lakes area toward the north-western recessing margin, that is, between the
438 Rocky Mountains and the LIS, encompassing the Mississippi and Missouri provinces. The
439 grainsize data (e.g., decreasing in the grain-size mode) suggest an increasing in the supplied
440 of fine-grained sediment to the GOM in Unit 2 (Figs. 10 and 11), in agreement with terrestrial
441 records showing that deglacial megafloods deeply eroded clay-rich terrace deposits along
442 upper Mississippi River tributaries (Knox, 1996), additionally, the subsequent incision of the
443 Mississippi River tributaries also supplied fine sediment to the fluvial suspended load

(Rittenour et al., 2007). Geochemical data, compared with the Al-normalized metal concentrations from the Mississippi drainage area (Gustavsson et al., 2001), give new evidences on the provenance of the detrital fraction during the meltwater episode. Thus, the high V/Al, Fe/Al, (Gd/Yb)n ratios, which cannot be attributed to authigenic/diagenetic processes because of linear relationships between these proxies and Al (Fig. 8), also pinpoint the northwestern province as the main detrital contributor during these events (Gustavsson et al., 2001). The low Ti/Al, Th/Al, K/Al, La/Al, Y/ Al and Total REE/Al ratios (Figs. 8 and 9) suggest a significantly reduced contribution of the northeast cratonic province. This period of high meltwater supply is also linked with the occurrence of organic layers previously described in the northwest GOM (Tripsanas et al., 2007). The laminations observed in Pigmy Basin may then correspond to: (1) slight stratification in the deep part of the basin as described for the Orca Basin (Tribovillard et al., 2009); or (2) an enhanced oxygen consumption related to increased terrigenous particles flux (organic and mineral) (e.g., Leventer et al., 1983; Meckler et al., 2008). However, there are no geochemical evidences of strong modifications of the redox conditions in the Pigmy Basin that did not undergo oxygen-restricted conditions. On the other hand, in Fig. 5 the MS values are quite low in Unit 2. It is noteworthy also that these low values correspond exactly with a high Fe/Al ratio (Fig. 9) and with a break in laminations (Fig. 1c). This could be discussed in terms of redox conditions. When oxygen levels decrease and other electron acceptors are required for organic matter degradation, magnetite-like iron – which is the dominant magnetic mineral in the Pigmy Basin sediments (King, 1986) – is reduced to Fe(II), which subsequently yields low MS values (e.g., Bloemendal et al., 1992). In summary, our results suggest that Unit 2 corresponds to the most intense meltwater pulse from the southwest margin of the LIS, remobilizing clay-rich terrace deposits from the northwest part of the Mississippi and Missouri river watershed (Knox, 1996). It is synchronous with the most intense period of freshwater discharge as previously described or modeled (Licciardi et al., 1999; Tarasov and Peltier, 2005), which occurred as the LIS was retreating progressively northward. This retreat yielded to the formation of numerous large glacial lakes between the ice margin and former moraines (Teller, 1990), which delivered large amounts of freshwater and sediment when their outlets incised their substratum (Teller et al., 2005; Fisher et al., 2006).

Unit 3 displays mineralogical and geochemical characteristics similar to those of Unit 1, which suggests similar provenance of the detrital supply. The clay composition indicates a re-start of contributions from the northeast province as the LIS was withdrawn from its

477 southern extent. The main discrepancy concerns the grain-size distribution that is mainly fine
478 and cohesive whereas Unit 1 was mostly coarse-grained. We propose that Unit 3 corresponds
479 to the late phase of the Meltwater Spike with reduced erosional processes.

480 This deglacial megafloods interval characterized in the Pigmy Basin (core MD02-
481 2553) is also supported by contemporaneous spikes observed in proxies of flood erosion
482 intensity (reworked nannofossils, siliciclastic grain-size, clay minerals) from the Orca Basin
483 cores (Fig. 11a,c–f), and by net accumulation rates of sedimentary organic carbon from the
484 Pigmy Basin (DSDP site 619) (Fig. 11g). It is important to emphasize that the difference in
485 the timing of peak meltwater discharge observed in the different sedimentary records most
486 likely reflects uncertainties in the individual core chronologies (e.g., Fig. 11e,f).

487 To summarize, our sedimentological and geochemical proxies allow differentiating
488 various phases of terrigenous supply originating from different source areas according to the
489 location in the time of the southern edge of LIS ice melting lobes.

490

491 *5.3. Sedimentary regime during the Pleistocene/Holocene transition (12.9–10 cal ka BP)*

492 Our results reveal that a major modification of the sedimentary regime occurred at
493 12.9 ka in the Pigmy Basin (Unit 4). The greater abundance of foraminifers in the uppermost
494 part of the core, based in the sedimentological descriptions of the core (Fig. 1c), suggests an
495 increased in the autochthonous biogenic contribution as the terrigenous input progressively
496 diminished. The higher CaCO3 concentration during this interval (Fig. 5) confirms this
497 increase in biogenic productivity probably related to warmer sea-surface temperature (SST)
498 evidenced in the Orca Basin (Flower et al., 2004). Warmer SST may reflect a decreased
499 seasonal influence of cold continental air masses over the GOM as the glacial shoreline
500 retreated over the Louisiana slope (Flower et al., 2004) or may alternatively be controlled by
501 insolation (Ziegler et al., 2008). Our results (notably, C/N ratio and Rock–Eval Pyrolysis) also
502 indicate that the organic matter is mainly of marine origin, in agreement with the proposed
503 increase in productivity and consistently with previous observations in the Pigmy Basin
504 (Jasper and Gagosian, 1990; Jasper and Hayes, 1993) and Orca Basin (Meckler et al., 2008;
505 Tribovillard et al., 2008, 2009; Sionneau et al., in revision).

506 The reduced terrigenous contribution is confirmed by the low sedimentation rate
507 observed after 12.9 ka (<25 cm/ka) in the Pigmy Basin. The grain-size distribution suggests
508 that the Mississippi River discharge capacity was significantly reduced, especially during the

Younger Dryas, in agreement with previous hypothesis (Brown and Kennett, 1998; Licciardi et al., 1999; Teller et al., 2005). The specific clay composition indicates the contribution of the south-eastern province to the sedimentation in the Pigmy Basin after 12.9 ka, as also observed in the sediment from the Orca Basin (Sionneau et al., in revision). All these observations confirm the hypothesis of a modification of the fluvial regime after 12.9 ka in which all meltwater discharges from the LIS are retained in proglacial lakes before entering the Mississippi River. Such a mechanism may trap coarse detrital fractions in proximal lakes and damp out any seasonal variations (Bettis et al., 2008).

During the early Holocene (after 11.5 ka), the grain-size distribution suggest modification of the sedimentary regime in the Pigmy Basin (e.g., Fig. 10e) synchronous with evidences of Mississippi River discharge linked to Lake Agassiz overflows (Licciardi et al., 1999; Teller et al., 2002, 2005). In the GOM, these meltwater events are evidenced on the Louisiana slope (MWF-5; Aharon, 2003; Fig. 11b) and Orca Basin (Meckler et al., 2008; Fig. 11e), but are not significantly recorded in other GOM cores (Marchitto and Wei, 1995; Brown and Kennett, 1998; Flower et al., 2004; Sionneau et al., in revision). In this context the absence of any major changes in clay mineral and geochemical records suggest that inflows were of reduced importance and unable to carry significant detrital loads (Sionneau et al., in revision) or alternatively that these detrital inputs correspond to the remobilization of stored glacigenic sediments as the Mississippi River got adjusted to the postglacial hydrologic regime (Knox, 1996; Brown and Kennett, 1998).

6. Summary and conclusions

Our multiproxy record from the Pigmy Basin in the northern GOM reveal large variations in the terrigenous input over the last deglaciation, which are likely associated with the Laurentide Ice Sheet (LIS) melting history and the Mississippi River discharge.

Four main sedimentological units can be distinguished upon their mineralogical and geochemical contents. Geochemical data indicate that sedimentation is mainly terrigenous in the Pigmy Basin, with no detectable authigenic processes, being strictly detrital (Units 1–3) during the deglaciation (15–12.9 cal ka BP) whereas significant biogenic contribution (Unit 4) is observed during the Younger Dryas and early Holocene (12.9–10 cal ka BP). Similarly, organic compounds are mostly terrigenous during thedeglaciation whereas they display a higher marine influence in the early Holocene.

Clay mineralogy and rare earth element distribution reveal that sedimentation in the Pigmy Basin is mainly controlled by detrital inputs from the Mississippi River watershed with major contribution of the north-western part and minor supplies from the northeastern province. Most proxies display stair-step pattern suggesting drastic modifications in both hydrodynamic and sediment provenance. These modifications are interpreted to result from changes in the Mississippi River floods caused by LIS meltwater discharges. Over the studied interval both ice sheet margin instabilities and ice lobe fluctuations modified meltwater provenance and caused the main drainage to be repeatedly rerouted eastward or northward, leading to specific stair-step pattern meltwater discharges in the GOM. A well-known modest surge of glacial meltwater (Melwater Spike or Meltwater Flow) is recorded by the deposition of sedimentological Units 1–3. Our sedimentological data provide new constraints on the synopsis of this major meltwater episode. The Meltwater Spike displays three distinct phases:

– Specific clay mineral and grain-size distributions suggest that meltwater originated from almost all the southern margin of the LIS and that erosion processes of the main Mississippi River channel were rather important during the early phase of the Meltwater Spike. Unit 1 is thus interpreted as the record the initial erosive flood, which may correspond to the proglacial lake Wisconsin outburst (14.9 cal ka BP).

– Unit 2 is characterized by major modifications of provenance of the main detrital supply suggesting a westward shift of the main outflow from the Great lakes area toward the recessing north-western margin. According to geochemical evidences, the organic-rich laminations observed in the Pigmy Basin are interpreted as the result of enhanced detrital particles flux rather than water stratification in the deep part of the basin. Unit 2 records the paroxysmal phase of the meltwater pulse originating from the southwest margin of the LIS while retreating.

– Unit 3 corresponds to the late phase of the Meltwater Spike with reduced erosional processes. The clay composition indicates the onset of contributions from the northeast province as the LIS was withdrawn from its southern extent.

A major modification of the sedimentary regime – increase in biogenic contribution and decrease in terrigenous supply – occurred at ca 12.9 cal ka BP in the Pigmy Basin (Unit 4). These modifications mirrors the average changes in the magnitude of the sedimentation rates from about 200 to 25 cm/ka, which is consistent with major reduction of meltwater flow during this time, and may reveal differences due to clastic dilution. Geochemical and

sedimentological proxies suggest an increase in productivity probably related to warmer sea-surface temperature controlling by either seasonality or insolation. The grain-size distribution also suggests that the Mississippi River discharge capacity was significantly reduced, especially during the Younger Dryas whereas specific clay composition (e.g., kaolinite) indicates the contribution of the south-eastern province. These observations confirm a modification of the fluvial regime where all meltwaters were trapped in proglacial lakes before entering the Mississippi River.

During the early Holocene (after 11.5 ka) some minor modifications of the sedimentary regime may reflect episodic Mississippi River discharge linked to Lake Agassiz overflows. But the absence of any major changes in clay mineral and geochemical records suggest that inflows were of reduced importance in agreement with the lack of significant hydrological modifications in the GOM. Alternatively, these detrital inputs may thus correspond to the remobilization of stored glacigenic sediments as the Mississippi River got adjusted to the postglacial hydrologic regime.

Acknowledgements

We thank Yvon Balut, the Institut Paul-Emile Victor (IPEV), the officers and crew of the R/V Marion Dufresne and the IMAGES program for core collection. This study was financially supported by: (1) the UMR Geéosystèmes of the Université Lille 1 (France); and (2) the Program Alban, the European Union Program of High Level Scholarships for Latin America, scholarship No. E06D100913VE.We thank the technical staff of the Geéosystèmes lab: Léa-Marie Emaille, Laurence Debeauvais, Deny Malengros, Philippe Recourt & Deborah Ponleve. The authors are grateful to François Baudin (Université Pierre et Marie Curie – Paris 6) for performing the Rock–Eval analyses. VBR thanks Laurent Labeyrie for initiating the IMAGES PAGE cruise. Thanks to the two anonymous reviewers for improving this manuscript through careful review, and to Neil Glasser for his editorial work.

References

Aharon, P., 2003. Meltwater flooding events in the Gulf of Mexico revisited: Implications for rapid climate changes during the last deglaciation. Paleoceanography 18, 1079, doi: 10.1029/2002PA000840.

604 Aharon, P., 2006. Entrainment of meltwaters in hyperpycnal flows during deglaciation
605 superfloods in the Gulf of Mexico. Earth and Planetary Science Letters 241, 260-270.

606 Alley, R.B., 2000. The Younger Dryas cold interval as viewed from central Greenland.
607 Quaternary Science Reviews 19, 213-226.

608 Bard, E., 1988. Correction of accelerator mass spectrometry C-14 ages measured in
609 planktonic foraminifera: paleoccanography implications. Paleoceanography 3, 634–645.

610 Bettis, E.A., Benn, D.W., Hajic, E.R., 2008. Landscape evolution, alluvial architecture,
611 environmental history, and the archaeological record of the Upper Mississippi River
612 Valley. Geomorphology 101, 362-377.

613 Bouma, A.H., 1981. Depositional sequences in clastic continental slope deposits, Gulf of
614 Mexico. Geo-Marine Letters 1, 115–121.

615 Bouma, A., Coleman, J., 1986. Intraslope basin deposits and relation to continental shelf,
616 northern Gulf of Mexico. American Association of Petroleum Geologists Bulletin, v. 70,
617 no. 9, p. 1178.

618 Bouma, A.H., Stelting, C.E., Leg 96 sedimentologists, 1986. Seismic stratigraphy and
619 sedimentary processes in Orca and Pigmy Basin. In Initial Reports of the Deep-Sea
620 Drilling Project. Leg 96. Bouma, A.H., Coleman, J.M., Meyer, A.W., et al., (Eds), pp.
621 563-576, Washington D.C., U.S. Government Printing Office.
622 doi:10.2973/dsdp.proc.96.128.1986.

623 online at http://www.deepseadrilling.org/96/volume/dsdp96_28.pdf

624 Bout-Roumazeilles, V., Cortijo, E., Labeyrie, L., Debrabant, P., 1999. Clay mineral evidence
625 of nepheloid layer contribution to the Heinrich layers in the Northwest Atlantic.
626 Palaeogeography, Palaeoclimatology, Palaeoceanography 146, 211-228.

627 Bout-Roumazeilles, V., Trentesaux, A., 2007. Sedimentologic analysis of cores, recovered
628 from the RV Marion Dufresne cruise in the Gulf of Mexico, chapter 5, July 2002, PAGE
629 127 Campaign. In: Winters, W.J., Lorenson, T.D., Paull, C.K. (Eds.), Initial Report of the
630 IMAGES VIII/PAGE 127 Gas Hydrate and Paleoclimate Cruise on the RV Marion
631 Dufresne in the Gulf of Mexico, 2–18 July 2002: U.S. Geological Survey Open-File
632 Report 2004-1358, one DVD. Online at http://pubs.usgs.gov/of/2004/1358/.

633 Broecker, W.S., Kennett, J.P., Flower, B.P., Teller, J.T., Trumbore, S., Bonani, G., Wolfli,
634 W., 1989. Routing of meltwater from the Laurentide Ice-Sheet during the Younger Dryas
635 cold episode. Nature 341, 318–321.

636 Brown, G., Brindley, G.W., 1980. X-ray diffraction procedures for clay mineral identification,
637 in: Brindley, G.W., Brown, G. (Eds.), Crystal Structures of Clay Minerals and their X-ray
638 Identification. Mineralogical Society, London, pp. 305-359.

639 Brown, P.A., Kennett, J.P., 1998. Megaflood erosion and meltwater plumbing changes during
640 last North American deglaciation recorded in Gulf of Mexico sediments. Geology 26,
641 599–602.

642 Clark, P.U., Marshall, S.J., Clarke, G.K.C., Hostetler, S.W., Licciardi, J.M., Teller, J.T., 2001.
643 Freshwater forcing of abrupt climate change during the last glaciation. Science 293, 283–
644 287.

645 Coleman, J.M., 1988. Dynamic changes and processes in the Mississippi River delta.
646 Geological Society of America Bulletin 100, 999–1015.

647 Diegel, F.A., Karlo, J.F., Schuster, D.C., Shoup, R.C., Tauvers, P.R., 1995. Cenozoic
648 structural evolution and tectono-stratigraphic framework of the northern Gulf coast
649 continental margin, in M. P. A. Jackson, D. G. Roberts, and S. Snelson, eds., Salt
650 tectonics: a global perspective: AAPG Memoir 65, p. 109–151.

651 Disnar, J.-R., Jacob, J., Morched-Issa, M., Lottier, N., Arnaud, F., 2008. Assessment of peat
652 quality by molecular and bulk geochemical analysis: application to the Holocene record of
653 the Chautagne marsh (Haute Savoie, France). Chemical Geology 254, 101–112.

654 Dyke, A.S., 2004. An outline of North American deglaciation with emphasis on central and
655 northern Canada, in Ehlers, J., Gibbard, P.L., (Eds), Quaternary Glaciations – Extent and
656 Chronology, Part II. Elsevier B.V., Amsterdam, pp. 373-424.

657 Elderfield, H., Upstill-Goddard, R., Sholkovitz, ER., 1990. The rare earth elements in rivers,
658 estuaries and coastal seas and their significance to the composition of ocean water.
659 Geochim. Cosmochim. Acta 54, 971–991.

660 Emiliani, C., Rooth, C., and Stripp, J.J., 1978. Late Wisconsin flood into the Gulf of Mexico.
661 Earth and Planetary Science Letters 41, 159–162

662 Espitalié, J., Deroo, G., Marquis, F., 1986. La pyrolyse Rock Eval et ses applications. Revue
663 de l'Institut Français du Pe´ trole 40 (B), 755–784.

664 Fisher, T.G., Lowell, T.V., and Loope, H.M., 2006. Alternative routing of Lake Agassiz
665 overfl ow during the Younger Dryas: New dates, paleotopography, and a re-evaluation:
666 Comment. Quaternary Science Reviews 25, 1137–1141.

667 Flower, B.P., Kennett, J.P., 1990. The Younger Dryas cool episode in the Gulf of Mexico.
668 Paleoceanography 5, 949–961.

669 Flower, B.P., Hastings, D.W., Hill, H.W., Quinn, T.M., 2004. Phasing of deglacial warming
670 and laurentide ice sheet meltwater in the Gulf of Mexico. Geology 32, 597–600.

671 Flocks, J., Swarzenski, P., 2007. Sediment collection from Orca and Pigmy Basins, Gulf of
672 Mexico, and analyses for texture and trace-metal concentrations, July 2002, PAGE 127
673 Campaign. In: Winters, W.J., Lorenson, T.D., Paull, C.K. (Eds.), Initial Report of the
674 IMAGES VIII/PAGE 127 Gas Hydrate and Paleoclimate Cruise on the RV Marion
675 Dufresne in the Gulf of Mexico, 2–18 July 2002: U.S. Geological Survey Open-File
676 Report 2004-1358, one DVD. online at http://pubs.usgs.gov/of/2004/1358/.

677 Goldstein, S.J., Jacobsen, S.B., 1988. Rare earth elements in river waters. Earth Planet. Sci.
678 Lett. 89, 35–47.

679 Gromet, L.P., Dymek, R.F., Haskin, L.A., Korotev, R.L., 1984. The North American shale
680 composite: its compilation, major and trace element characteristics. Geochimica et
681 Cosmochimica Acta 48, 2469–3482.

682 Gustavsson, N., Bølviken, B., Smith, D.B., Severson, R.C., 2001. Geochemical Landscapes of
683 the Conterminous United States – New Map Presentations for 22 Elements.

684 Hughen, K.A., Overpeck, J.T., Lehman, S.J., Kashgarian, M., Southon, J.R., Peterson, L.C.,
685 Alley, R., Sigman, D.M., 1998. Deglacial changes in ocean circulation from an extended
686 radiocarbon calibration. Nature 391 (6662), 65–68.

687 Hughen, K.A., Baillie, M.G.L., Bard, E., Beck, J.W., Bertrand, C.J.H., Blackwell, P.G., Buck,
688 C.E., Burr, G.S., Cutler, K.B., Damon, P.E., Edwards, R.L., Fairbanks, R.G., Friedrich,
689 M., Guilderson, T.P., Kromer, B., McCormac, G., Manning, S., Ramsey, C.B., Reimer,
690 P.J., Reimer, R.W., Remmele, S., Southon, J.R., Stuiver, M., Talamo, S., Taylor, F.W.,
691 van der Plicht, J.,Weyhenmeyer, C.E., 2004. Marine04 marine radiocarbon age
692 calibration, 0–26 cal kyr BP. Radiocarbon 46, 1059–1086.

693 Jasper, J.P., Gagosian, R.B., 1989a. Glacial–interglacial climatically-forced 13C variations of
694 sedimentary organic matter. Nature 342, 60–62.

695 Jasper, J.P., Gagosian, R.B., 1989b. Alkenone molecular stratigraphy in an oceanic
696 environment affected by glacial meltwater events. Paleoceanography 4, 603–614.

697 Jasper, J.P., Gagosian, R.B., 1990. The sources and deposition of organic matter in the late
698 Quaternary Pigmy Basin, Gulf of Mexico. Geochimica et Cosmochimica Acta 54, 1117–
699 1132.

700 Jasper, J.P., Hayes, J.M., 1993. Refined estimation of marine and terrigenous contributions to
701 sedimentary organic carbon. Global Biogeochemical Cycles 7, 451–461.

702 Joyce, E.J., Tjalsma, L.R.C., Prutzman, J.M., 1993. North American glacial meltwater history
703 for the past 2.3 m.y.: Oxygen isotope evidence from the Gulf of Mexico. Geology 21,
704 483–486.

705 Kennett, J.P., Shackleton, N.J., 1975. Laurentide ice sheet meltwater recorded in Gulf of
706 Mexico deep-sea cores. Science 188, 147–150.

707 King, J.W., 1986. Paleomagnetic and rock-magnetic stratigraphy of Pigmy Basin, Deep Sea
708 Drilling Project Site 619, Leg 96. In: Bouma, A.H., Coleman, J.M., Meyer, A.W., et al.
709 (Eds.), Init. Repts. DSDP, 96. U.S. Govt. Printing Office, Washington, pp. 677–684.

710 Knox, J.C., 1996. Late Quaternary Upper Mississippi River alluvial episodes and their
711 significance to the Lower Mississippi River system. Engineering Geology 45, 263–285.

712 Knox, J.C., 2000. Sensitivity of modern and Holocene floods to climate change. Quaternary
713 Science Reviews 19, 439–457.

714 Lawrence, M.G., Greig, A., Collerson, K.D., Kamber, B.S., 2006. Rare earth element and
715 yttrium variability in South East Queensland waterways. Aquatic Geochemistry 12, 39–
716 72.

717 Leventer, A., Williams, D.F., Kennett, J.P., 1982. Dynamics of the Laurentide ice sheet
718 during the last deglaciation: evidence from the Gulf of Mexico. Earth and Planetary
719 Science Letters 59, 11-17.

720 Leventer, A., Williams, D.F., Kennett, J.P., 1983. Relationships between anoxia, glacial
721 meltwater and microfossil preservation in the Orca Basin, Gulf of Mexico. Mar. Geol. 53,
722 23–40.

723 Lewis, C.F.M., Teller, J.T., 2006. Glacial runoff from North America and its possible impact
724 on oceans and climate, chapter 28. In: Knight, P.G. (Ed.), Glaciers and the Environment.
725 Blackwell Publishing Ltd., Oxford, UK.

726 Licciardi, J.M., Teller, J.T., Clark, P.U., 1999. Freshwater routing by the Laurentide ice sheet
727 during the last deglaciation, in Clark, P.U., et al., eds., Mechanisms of global climate
728 change at millennial time scales: American Geophysical Union Geophysical Monograph
729 112, p. 177–201.

730 Marchitto, T.M., Wei, K.Y., 1995. History of Laurentide meltwater flow to the Gulf of
731 Mexico during the last deglaciation, as revealed by reworked calcareous nannofossils.
732 Geology 23, 779–782.

733 Meckler, A.N., 2006. Late Quaternary changes in nitrogen fixation and climate variability
734 recorded by sediments from the Gulf of Mexico and the Caribbean Sea. PhD Thesis ETH
735 Zürich N° 16811, 156 p.

736 online at http://www.up.ethz.ch/people/former/nmeckler/PhD_Meckler.pdf

737 Meckler, A.N., C.J. Schubert, P.A. Hochuli, B. Plessen, D. Birgel, B.P. Flower, K.-U.
738 Hinrichs, and Haug, G.H., 2008. Glacial to Holocene terrigenous organic matter input to
739 sediments from Orca Basin, Gulf of Mexico – a combined optical and biomarker
740 approach. Earth and Planetary Science Letters 272, 251-263.

741 Meyers, P.A., 1997. Organic geochemical proxies of paleoceanographic, paleolimnologic, and
742 paleoclimatic processes. Org. Geochem. 27, 213–250.

743 Nürnberg, D., Ziegler, M., Karas, C., Tiedemann, R., Schmidt M.W., 2008. Interacting Loop
744 Current variability and Mississippi River discharge over the past 400 kyr. Earth and
745 Planetary Science Letters 272, 278-289.

746 Petschick, R. 2000. MacDiff 4.2 Manual. MacDiff [Online]. Available from World Wide
747 Web: <http://www.geologie.uni-frankfurt.de/Staff/Homepages/Petschick/RainerE.html>

748 Petschick, R., Kuhn, G., Gingele, F., 1996. Clay mineral distribution in surface sediments of
749 the South Atlantic: sources, transport, and relation to oceanography. Marine Geology 130,
750 203–229.

751 Piper, D.Z., 1974. Rare earth elements in the sedimentary cycle: a summary. Chemical
752 Geology 14, 285–304.

753 Poore, R.Z., Verardo, S., Caplan, J., Pavich, K., Quinn, T., in press. Planktic foraminiferal
754 relative abundance trends in the Gulf of Mexico Holocene sediments: Records of climate
755 variability, in Holmes, C., (Ed.), Gulf of Mexico, its origins, waters, biota, and human
756 impacts. Univ Texas Press.

757 Rittenour, T.M., Blum, M.D., Goble, R.J., 2007. Fluvial evolution of the lower Mississippi
758 River valley during the last 100 k.y. glacial cycle: response to glaciation and sea-level
759 change. Geological Society of America Bulletin 119, 586–608.

760 Rühlemann, C., Mulitza, S., Lohmann, G., Paul, A., Prange, M., Wefer, G., 2004.
761 Intermediate depth warming in the tropical Atlantic related to weakened thermohaline
762 circulation: combining paleoclimate data and modelling results for the last deglaciation.
763 Paleoceanography 19, PA1025. doi:10.1029/2003PA000948.

764 Schroeder, C.J., 1983. Changes in Benthic Foraminifer Assemblages across the
765 Holocene/Pleistocene Boundary, Sites 619, 620, 621, 622, and 624, Deep Sea Drilling
766 Project Leg 96. In: Bouma, A.H., Coleman, J.M., Meyer, A.W., et al., (Eds.), Initial
767 Reports of the Deep-Sea Drilling Project. Leg 96. Washington D.C., U.S. Government
768 Printing Office, pp. 631–642. doi:10.2973/dsdp.proc.96.133.1986.

769 Sionneau, 2008a. Transferts Continent – Océan : Enregistrement du dernier cycle climatique
770 par les sédiments terrigènes du Golfe du Mexique. PhD thesis, Université Lille 1. 322 p.

771 Sionneau, T., Bout-Roumazeilles, V., Biscaye, P.E., van Vliet-Lanoë, B., Bory, A., 2008b.
772 Clay Mineral distributions in and around Mississippi River watershed and Northern Gulf
773 of Mexico: Sources and transport patterns. Quaternary Science Reviews 27, 1740-1751.

774 Sionneau, T., Bout-Roumazeilles, V., Flower, B.P., Bory, A., Tribovillard, N., Kissel, C., Van
775 Vliet-Lanoë, B., Montero-Serrano, J.C., submitted for publication. On the provenance of
776 freshwater pulses in the Gulf of Mexico during the last deglaciation: Evidence from grain
777 size and clay mineralogy.

778 Sperazza, M., Moore, J.E., Hendrix, M.S., 2004. High-resolution particle size analysis of
779 naturally occurring very fine-grained sediment through laser diffractometry. Journal of
780 Sedimentary Research 74, 736–743.

781 Spero, H. J., Williams, D.F., 1990. Evidence for seasonal low salinity surface waters in the
782 Gulf of Mexico over the last 16,000 years. Paleoceanography 5, 963–975.

783 Stocker, T.F., Wright, D.G., 1996. Rapid changes in ocean circulation and atmospheric
784 radiocarbon. Paleoceanography 11 (6), 773–795.

785 Stuiver, M., Reimer, P.J., 1993. Extended C-14 data-base and revised calib 3.0 C-14 age
786 calibration program. Radiocarbon 35, 215–230.

787 Tanaka, K., Akagawa, F., Yamamoto, K., Tani, Y., Kawabe, I., Kawai, T., 2007. Rare earth
788 element geochemistry of Lake Baikal sediment: its implication for geochemical response
789 to climate change during the Last Glacial/Interglacial transition. Quaternary Science
790 Reviews 26, 1362–1368.

791 Tarasov, L., Peltier, W.R., 2005. Arctic freshwater forcing of the Younger Dryas cold
792 reversal: Nature 435, 662–665.

793 Teller, J.T., 1990. Volume and routing of late-glacial runoff from the southern Laurentide Ice
794 Sheet. Quaternary Research 34, 12-23.

795 Teller, J.T., Leverington, D.W., Mann, J.D., 2002. Freshwater outbursts to the oceans from
796 glacial Lake Agassiz and their role in climate change during the last deglaciation.
797 Quaternary Science Reviews 21, 879–887.

798 Teller, J.T., Boyd, M., Yang, Z.R., Kor, P.S.G., Fard, A.M., 2005. Alternative routing of Lake
799 Agassiz overflow during the Younger Dryas: new dates, paleotopography, and a
800 reevaluation. Quat. Sci. Rev. 24, 1890–1905.

801 Tieh, T.T., Stearns, S.V., Presley, B.J., 1983. Mineralogy and Incipient Diagenesis of Pigmy
802 Basin Sediments, Hole 619, Deep Sea Drilling Project Leg 96. In Initial Reports of the
803 Deep-Sea Drilling Project. Leg 96. Bouma, A.H., Coleman, J.M., Meyer, A.W., et al.,
804 (Eds), pp. 631-642, Washington D.C., U.S. Government Printing Office.
805 doi:10.2973/dsdp.proc.96.129.1986.

806 Online at http://www.deepseadrilling.org/96/volume/dsdp96_29.pdf

807 Tribovillard, N., Algeo, T., Lyons, T.W., Riboulleau, A., 2006. Trace metals as paleoredox
808 and paleoproductivity proxies: an update. Chem. Geol. 232, 12–32.

809 Tribovillard, N., Bout-Roumazeilles, V., Algeo, T.J., Lyons, T., Sionneau, T., Montero-
810 Serrano, J.C., Riboulleau, A., Baudin, F., 2008a. Paleodepositional conditions in the Orca
811 Basin as inferred from organic matter and trace metal contents. Marine Geology 254, 62-
812 72.

Tribovillard, N., Bout-Roumazeilles, V., Sionneau, T., Montero-Serrano, J.C., Riboulleau, A., Baudin, F., 2008b (in press). Does a strong pycnocline impact organic-matter preservation and accumulation in an anoxic setting? The case of the Orca Basin, Gulf of Mexico. Comptes Rendus Geosciences, doi:10.1016/j.crte.2008.10.002.

Tripsanas, E.K., Bryant, W.R., Slowey, N.C., Bouma, A.H., Karageorgis, A.P., Berti, D., 2007. Sedimentological history of Bryant Canyon area, northwest Gulf of Mexico, during the last 135 kyr (Marine Isotope Stages 1-6): A proxy record of Mississippi River discharge. Palaeogeography Palaeoclimatology Palaeoecology, 246: 137-161.

Van derWeijden, C.H., 2002. Pitfalls of normalization of marine geochemical data using a common divisor. Mar. Geol. 184, 167–187.

Wedepohl, K.H., 1971. Environmental influences on the chemical composition of shales and clays. In: Ahrens, L.H., Press, F., Runcorn, S.K., Urey, H.C. (Eds.), Physics and Chemistry of the Earth. Pergamon, Oxford, pp. 305–333.

Wedepohl, K.H., 1991. The composition of the upper Earth's crust and the natural cycles of selected metals. In: Merian, E. (Ed.), Metals and Their Compounds in the Environment. VCH-Verlagsgesellschaft, Weinheim, pp. 3–17.

Ziegler, M., Nürnberg, D., Karas, C., Tiedemann, R., Lourens, L.J., 2008. Persistent summer expansion of the AtlanticWarm Pool during glacial abrupt cold events. Nature Geoscience 1 (9), 601–605.

833 **Figure caption**

834 Table 1 – Radiocarbon ages for MD02-2553

Lab number or reference	Core depth (cm)	Species	^{14}C AMS Age (ca)	^{14}C Error (± year)	Calibrated age (median, ca BP)	Calibarted error (± year, 1 sigma)
Poore et al. (in press)	350,5	Mixed planktic foraminifers	9170	40	9989	89
	375,5		9905	40	10810	112
	390,5		10400	40	11364	61
	409,5		10888	40	12529	81
	424,5		11455	40	12956	44
Poz-24558	640,0	*Globigerinoides ruber*	12580	80	14034	98
Poz-24559	932,0		12960	80	14769	195

835

836

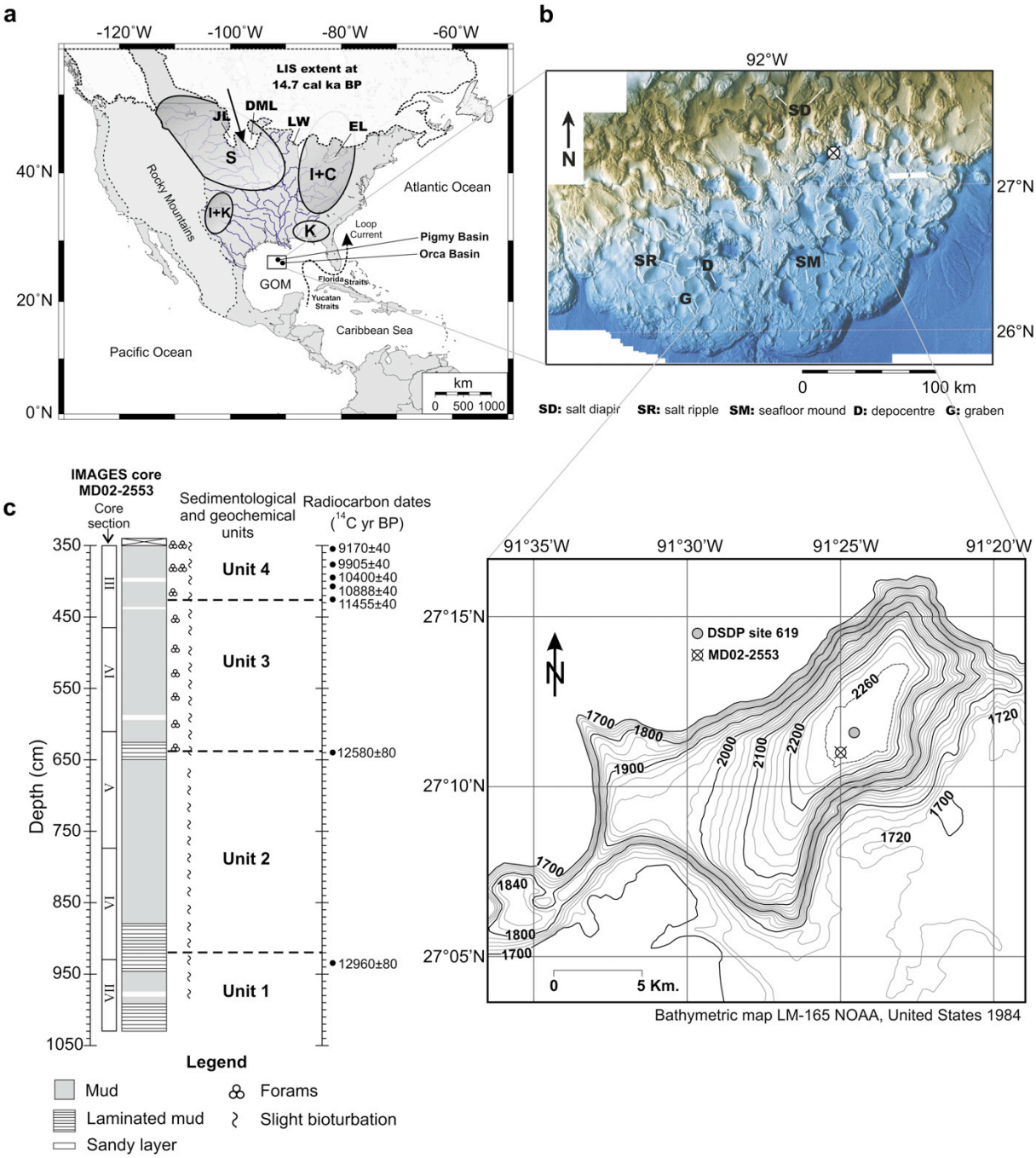

Fig. 1. (a) Map of North America with the extent of the Laurentide Ice Sheet during the last deglaciation (14.7 cal ka BP) (Dyke, 2004) showing the main continental clay minera provinces (Sionneau et al., 2008); S: smectite, I: illite, C: chlorite, K: kaolinite, GOM: Gulf of Mexico, JL: James glacial lobe, DML: Des Moines glacial lobe, LW: Lake Wisconsin, EL: Erie Lake. (b) Morphological map of the seafloor in the northern Gulf of Mexico (Diegel et al., 1995), and bathymetric map of the Pigmy Basin showing locations of sediment cores MD02-2553 and DSDP 619; contours in meters. (c) Lithological log of core MD02-2553 between 350 and 1050 cm showing the sedimentological and geochemical units defined in this study and radiocarbon ages; Roman numerals in column on far left represent the different core sections.

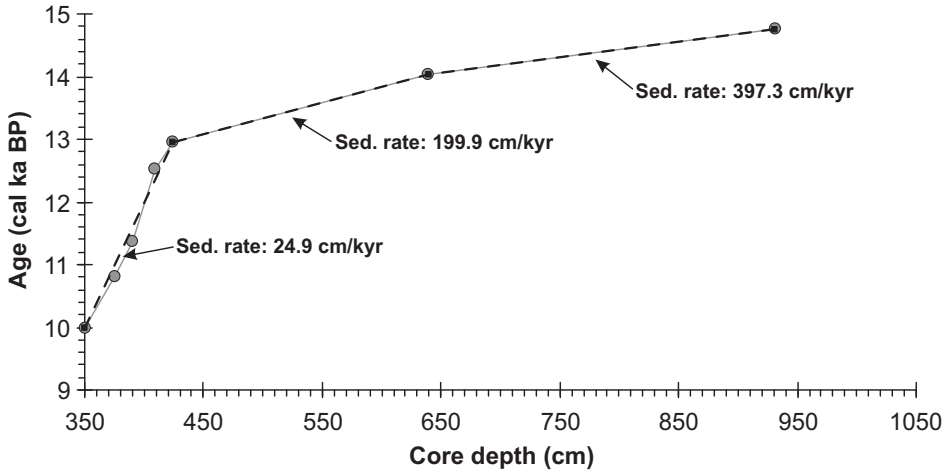

847

848 Fig. 2. Age model for core MD02-2553 based on 7 AMS 14C dates (gray dots) from both
849 Globigerinoides ruber and mixed planktic foraminifers, converted to calendar ages (see text). Depth in
850 centimeters was converted to calendar age by linear interpolation between the four dates at 350.5,
851 424.5, 640 and 932 cm (dotted line with black squares).

852

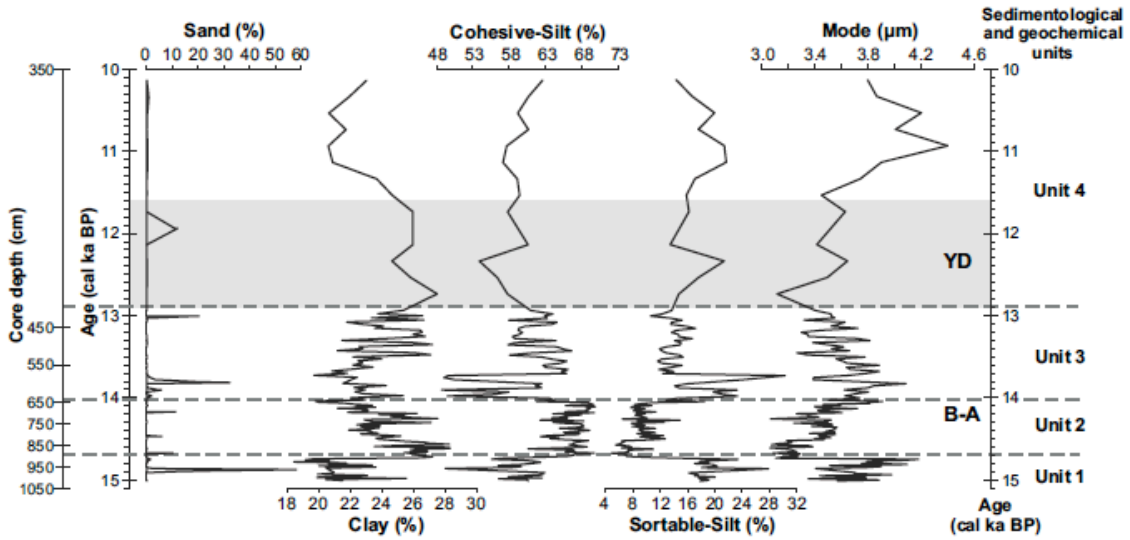

853

854 Fig. 3. Grain-size distribution (grain-size classes in %, and mode in mm). The Younger Dryas (YD)
855 from 12.9 to 11.6 ka (shaded) and Bølling–Allerød warming (B–A) from 15.4 to 12.9 ka are indicated.

856

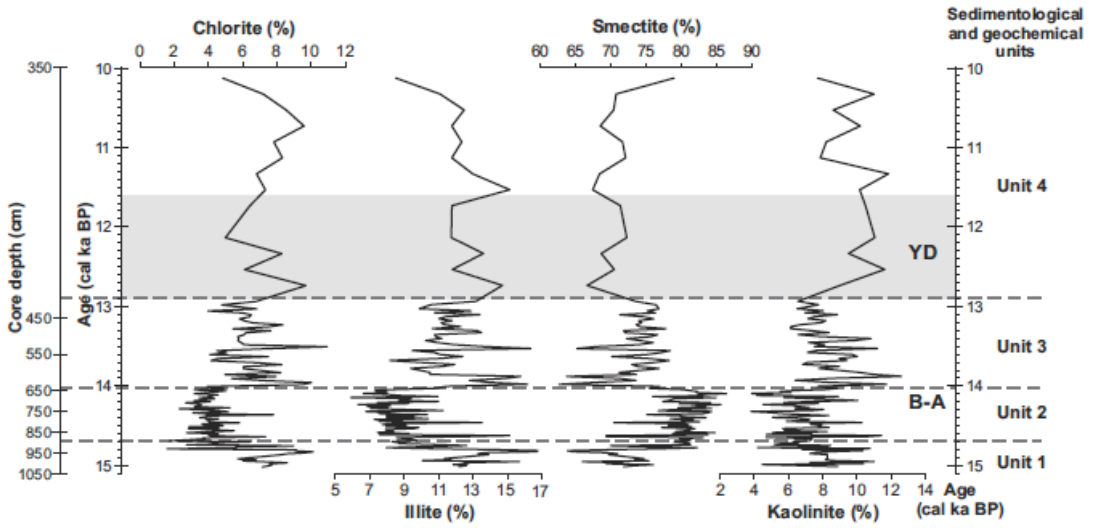

857

858 Fig. 4. Clay mineral variations. The Younger Dryas (YD) from 12.9 to 11.6 ka (shaded) and Bølling–
859 Allerød warming (B–A) from 15.4 to 12.9 ka are indicated.

860

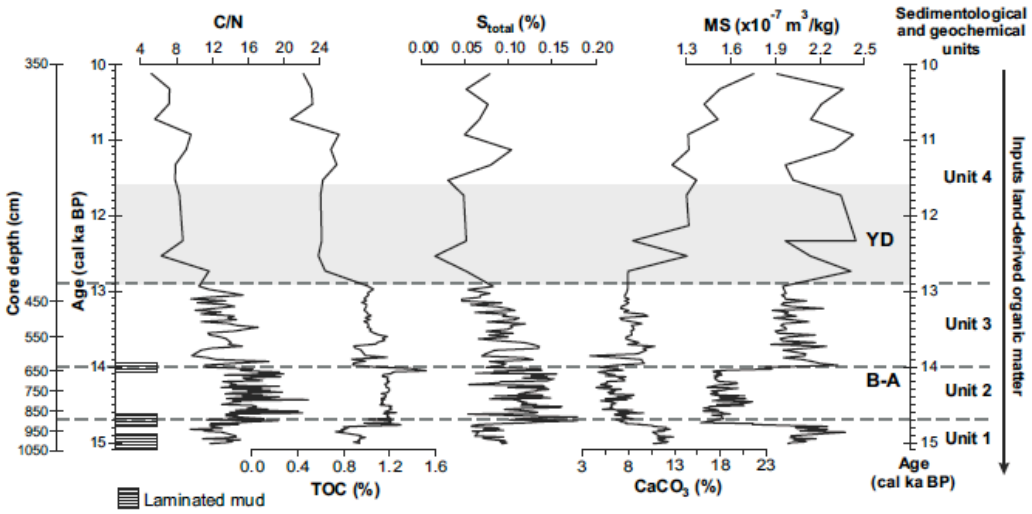

861

862 Fig. 5. C/N ratio, TOC, Stotal and carbonate (CaCO3) concentrations (%), and magnetic susceptibility
863 (MS) values. The Younger Dryas (YD) from 12.9 to 11.6 ka (shaded) and Bølling–Allerød warming
864 (B–A) from 15.4 to 12.9 ka are indicated.

865

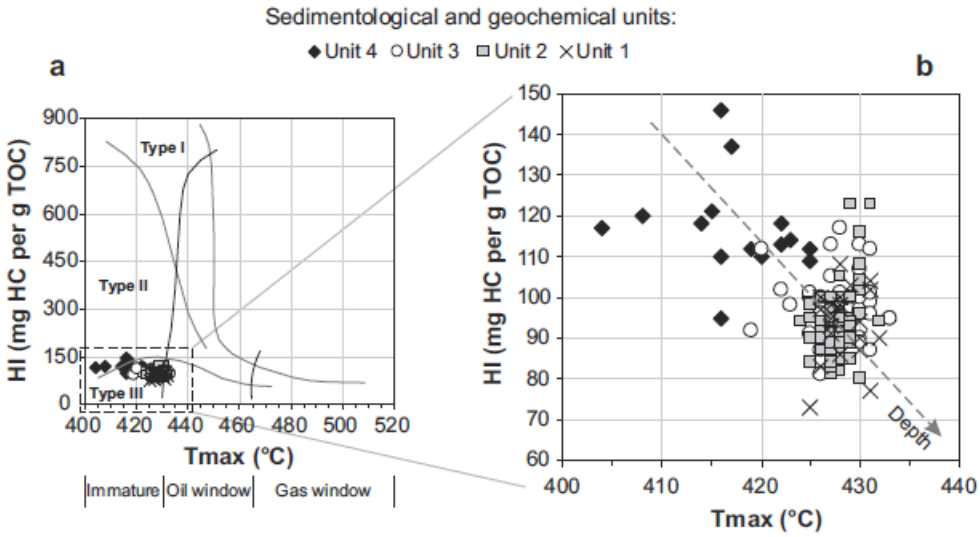

866

867 Fig. 6. Rock–Eval pyrolysis parameters. (a) TOC vs. Hydrogen Index (HI), (b) Tmax vs. HI crossplot
868 illustrating the origin and maturation state of the samples. The arrows on (a) and (b) show the general
869 tendency with sample depth below sea floor.

870

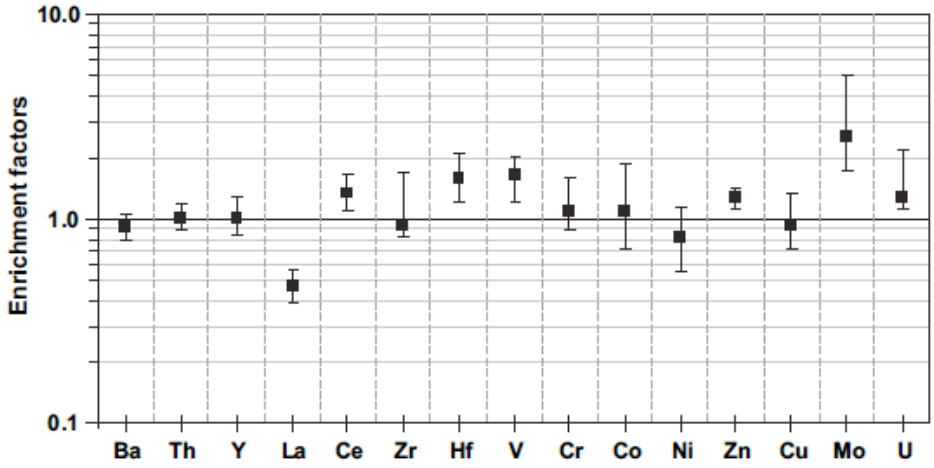

Fig. 7. Comparison of enrichment factor of some trace metals of core MD02-2553 (Pigmy Basin). The extent line of the boxes corresponds to the range of values (min–max) and the boxes to the average value. The horizontal line of the centre indicates the value for which there is no enrichment/depletion with regards to average shale composition.

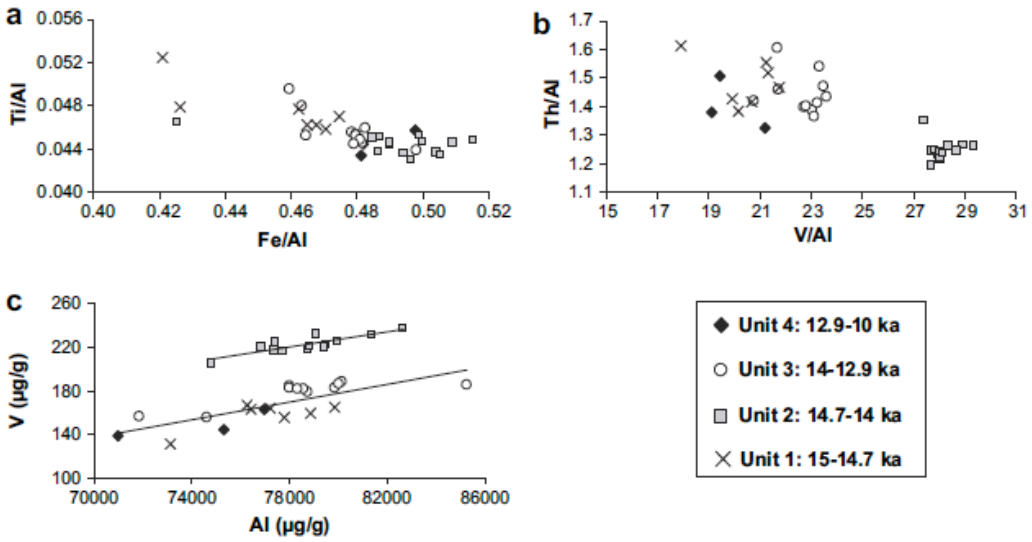

877

878 Fig. 8. (a) Ti/Al vs. Fe/Al, (b) Th/Al vs. V/Al, (c) V concentration vs. Al concentration for the studied
879 Pigmy samples.

880

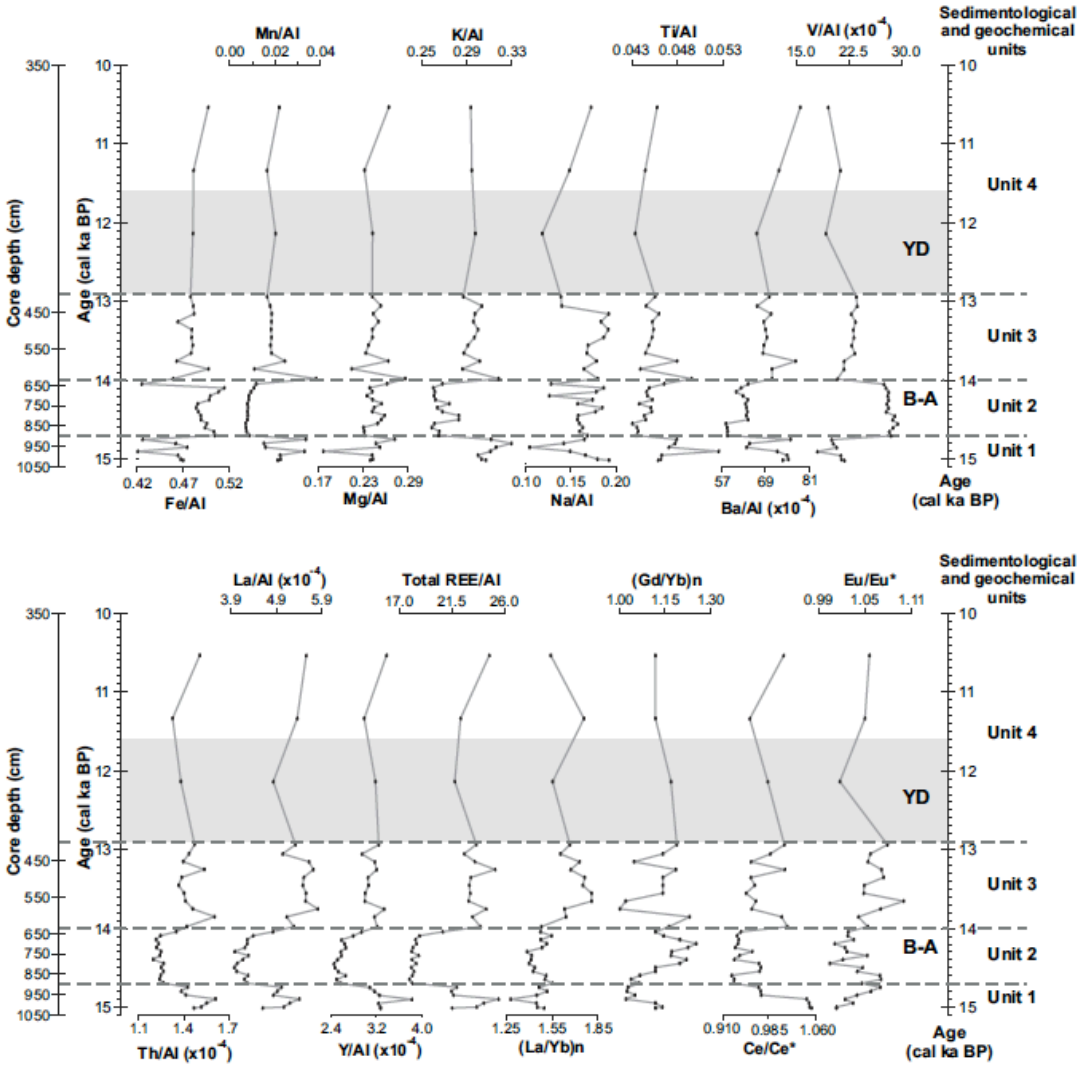

881

882 Fig. 9. Al-normalized elemental ratios: major, minor, traces and rare earth (REE) elements. The suffix
883 ‘‘n’’ denotes a NASC-normalized value (Gromet et al., 1984). The Ce and Eu anomalies are shown.
884 The Younger Dryas (YD) from 12.9 to 11.6 ka (shaded) and Bølling–Allerød warming (B–A) from
885 15.4 to 12.9 ka are indicated.

886

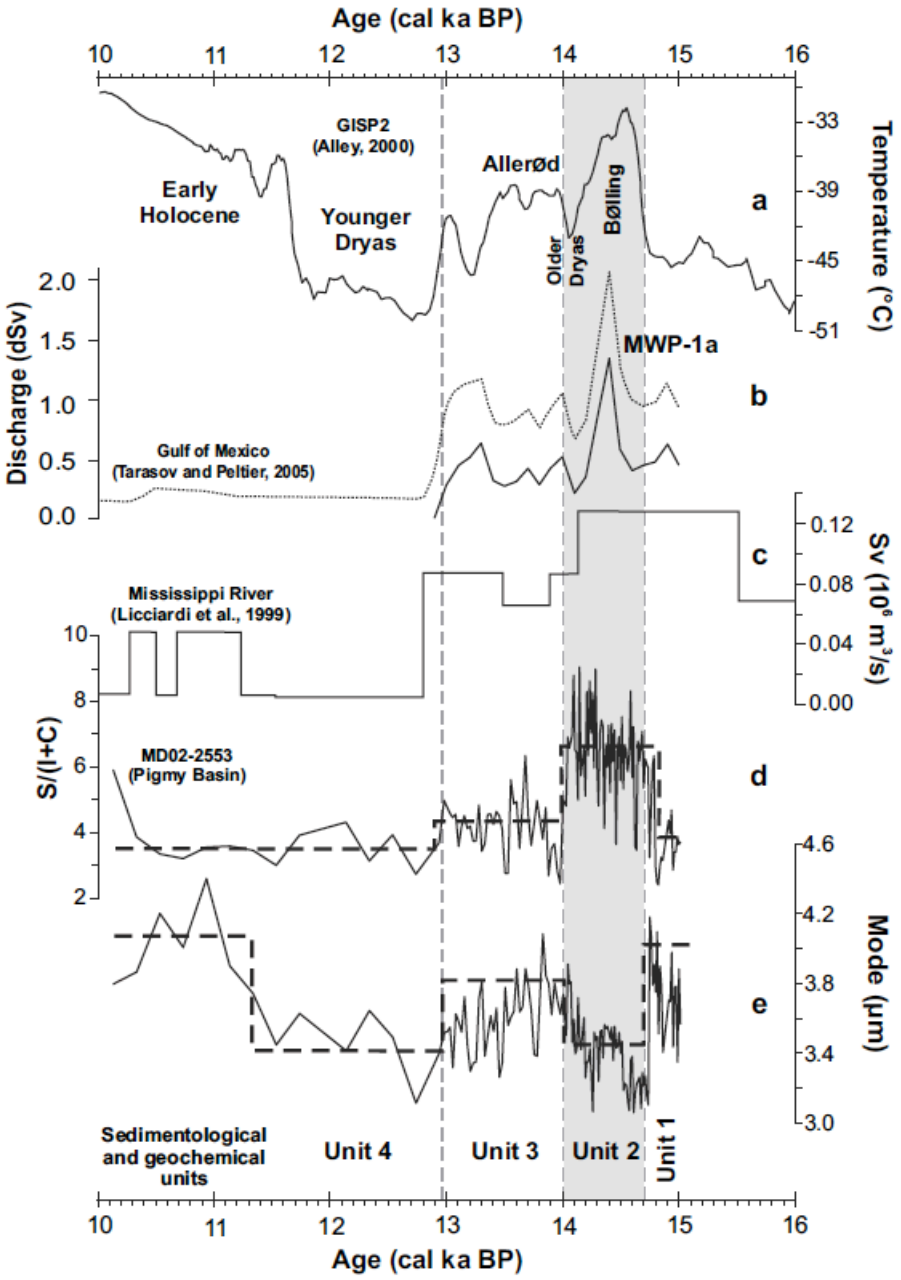

887

888 Fig. 10. Comparison of the sedimentological parameters of coreMD02-2553 (Pigmy Basin) with ice
889 proxy climate records and meltwater dischargemodels during 15–10 cal ka BP interval. (a) The
890 Greenland Ice Sheet Project 2 (GISP2) temperature (Alley, 2000). (b) Computed regional drainage
891 chronologies for theGulf ofMexico (1 dSv 1/4 105 m3/s) (Tarasov and Peltier, 2005); upper bound
892 (fine dotted line) denotes the 1s upper bound with the additional inclusion of precipitation over ice-
893 free land in the discharge calculation. (c) The meltwater discharge curve for the Mississippi River
894 (Licciardi et al., 1999). Sedimentary records in the Pigmy Basin: (d) clay mineral ratio S/(I + C), and
895 (e) grain-size mode (mm). The sedimentological and geochemical units defined in this study are
896 indicated. Shaded interval indicates the most intense meltwater pulse from the southwest margin of the
897 Laurentide Ice Sheet.

898

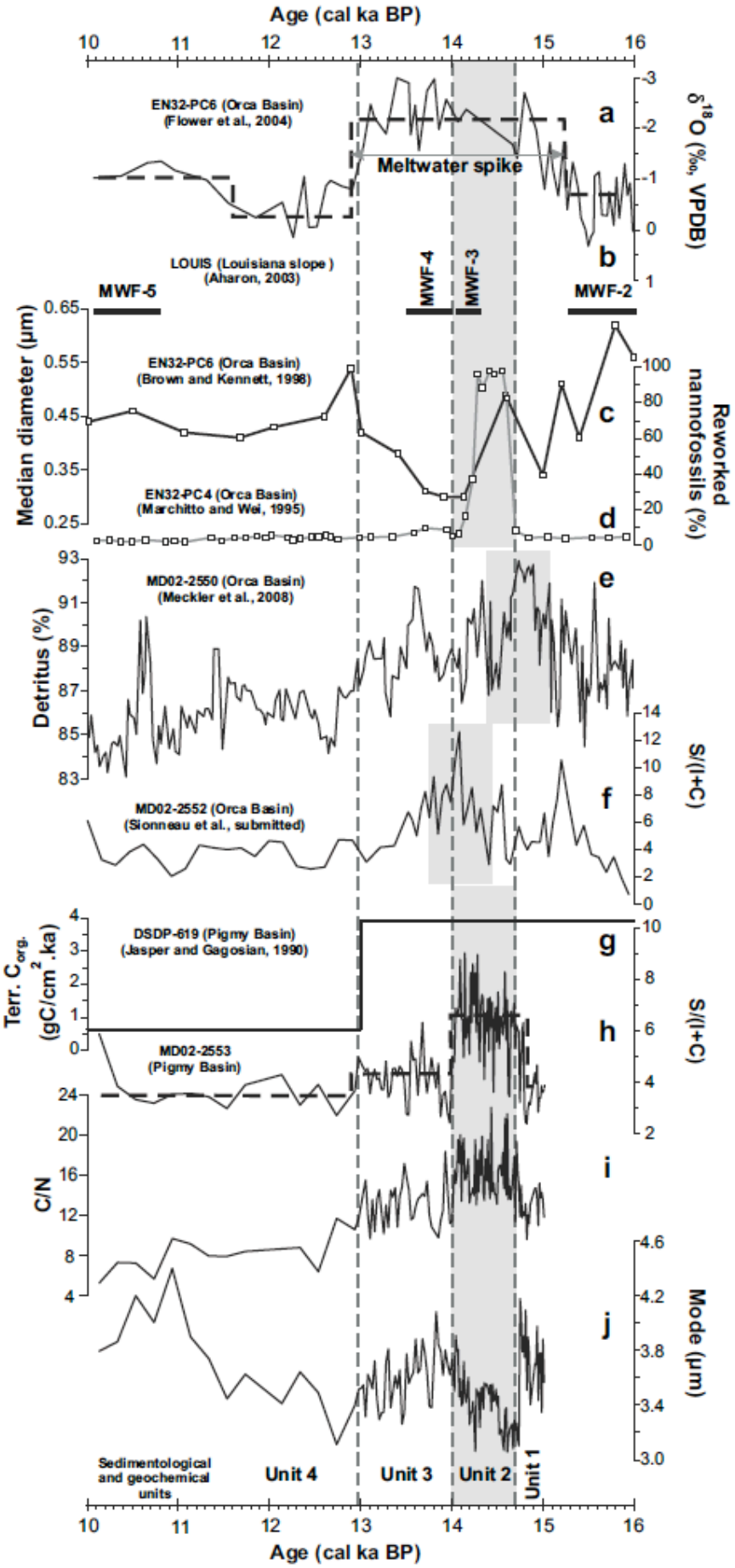
Age (cal ka BP)
EN32-PC6 (Orca Basin)
(Flower et al., 2004)
Meltwater spike
δ18O (‰, VPDB)
LOUIS (Louisiana slope)
(Aharon, 2003)
MWF-5
MWF-4
MWF-3
MWF-2
Median diameter (µm)
EN32-PC6 (Orca Basin)
(Brown and Kennett, 1998)
Reworked nannofossils (%)
EN32-PC4 (Orca Basin)
(Marchitto and Wei, 1995)
Detritus (%)
MD02-2550 (Orca Basin)
(Meckler et al., 2008)
S/(I+C)
MD02-2552 (Orca Basin)
(Sionneau et al., submitted)
Terr. Corg. (gC/cm2.ka)
DSDP-619 (Pigmy Basin)
(Jasper and Gagosian, 1990)
MD02-2553
(Pigmy Basin)
C/N
Mode (µm)
Sedimentological and geochemical units
Unit 4
Unit 3
Unit 2
Unit 1
Age (cal ka BP)

899

Fig. 11. Comparison of the sedimentological parameters of core MD02-2553 (Pigmy Basin) with proxy records of meltwater discharges of other GOM cores during 15–10 cal ka BP interval. (a) The d18O foraminifer records from Orca Basin core EN32-PC6 (Flower et al., 2004). (b) Bold line mark the successions of meltwater floods (MWF 2–5) recognized by Aharon (2003) in Louisiana slope (LOUIS) cores from northern GOM. Proxy records interpreted to represent meltwater flood erosion intensity and provenance records in the Orca Basin cores: (c) siliciclastic grain-size from core EN32-PC6 (Brown and Kennett, 1998), (d) percent reworked calcareous nannofossils as percent of total nannofossil assemblage from core EN32-PC4 (Marchitto and Wei, 1995), (e) percent of detritus from core MD02-2550; a proxy of terrigenous input (Meckler et al., 2008) and, (f) clay mineral ratio S/(I + C) from core MD02-2552 (Sionneau et al., in revision). Sedimentary records in the Pigmy Basin: (g) net accumulation rates (gC/cm2 ka) of terrigenous organic carbon (Corg.) from core DSDP site 619 (Jasper and Gagosian, 1990), (h) clay mineral ratio S/(I + C), (i) C/N ratio, and (j) grain-size mode (mm) from core MD02-2553 (this study). The sedimentological and geochemical units defined in this study are indicated. The original age model is used in all records with calibration of radiocarbon time scales to calendar years before present using CALIB 5.0.2 (Stuiver and Reimer, 1993) where needed. VPDB – Vienna Peedee belemnite. Shaded interval indicates the most intense meltwater pulse from the southwest margin of the Laurentide Ice Sheet.